AUTOMATED GLAND AND NUCLEI SEGMENTATION FOR GRADING OF PROSTATE AND BREAST CANCER HISTOPATHOLOGY

*Shivang Naik, Scott Doyle, Shannon Agner, Anant Madabhushi**

Rutgers, The State University of New Jersey
Department of Biomedical Engineering
Piscataway, New Jersey, USA 08854
E-mail: anantm@rci.rutgers.edu

Michael Feldman, John Tomaszewski

University of Pennsylvania
Department of Surgical Pathology
Philadelphia, Pennsylvania, USA 19104

ABSTRACT

Automated detection and segmentation of nuclear and glandular structures is critical for classification and grading of prostate and breast cancer histopathology. In this paper, we present a methodology for automated detection and segmentation of structures of interest in digitized histopathology images. The scheme integrates image information from across three different scales: (1) low-level information based on pixel values, (2) high-level information based on relationships between pixels for object detection, and (3) domain-specific information based on relationships between histological structures. Low-level information is utilized by a Bayesian classifier to generate a likelihood that each pixel belongs to an object of interest. High-level information is extracted in two ways: (i) by a level-set algorithm, where a contour is evolved in the likelihood scenes generated by the Bayesian classifier to identify object boundaries, and (ii) by a template matching algorithm, where shape models are used to identify glands and nuclei from the low-level likelihood scenes. Structural constraints are imposed via domain-specific knowledge in order to verify whether the detected objects do indeed belong to structures of interest. In this paper we demonstrate the utility of our glandular and nuclear segmentation algorithm in accurate extraction of various morphological and nuclear features for automated grading of (a) prostate cancer, (b) breast cancer, and (c) distinguishing between cancerous and benign breast histology specimens. The efficacy of our segmentation algorithm is evaluated by comparing breast and prostate cancer grading and benign vs. cancer discrimination accuracies with corresponding accuracies obtained via manual detection and segmentation of glands and nuclei.

***Index Terms*—** Prostate cancer, Breast cancer, Segmentation, Detection, Grading

1. INTRODUCTION

Over 200,000 new cases of prostate cancer and close to 200,000 new cases of breast cancer are predicted in the United States in 2008 (*American Cancer Society*). Currently, the diagnosis of prostate and breast cancer is done manually by visual analysis of tissue samples that have been obtained from a patient via biopsy. For prostate cancer, the Gleason grading scheme is used to quantify the degree of malignancy. In the case of breast cancer, the most popular grading scheme is Bloom-Richardson [1] for distinguishing between low-, high-, and intermediate grade cancers. Cancer grade is a key feature used to predict patient prognosis and in prescribing a treatment. Manual grading is time consuming and on account of its qualitative nature can lead to inter- and intra-observer variability [2], leading in turn to variable prognosis and suboptimal treatment.

In order to address the issues arising from manual cancer grading, our group has developed computer aided diagnosis (CAD) systems for automated grading of prostate and breast histology [3]. Our CAD methodology involves extraction of several hundred architectural, and morphological features derived from glands and nuclei which are manually segmented, a laborious and time-consuming process. Classification accuracies in discriminating intermediate grades of prostate and breast cancer were, however, above 90%.

In the interest of obtaining a fully automated grading scheme, it is imperative to be able to first automatically identify and segment histological structures. Nuclei segmentation has been attempted using basic fuzzy c-means clustering [4] and adaptive thresholding [5]. Other thresholding algorithms were investigated by Korde, et al. [6] for bladder and skin cell nuclear segmentation. However, thresholding leads to poor results when there is large variability in the histology staining. Other algorithms have been proposed using more complex techniques, such as an active contour scheme for pap-stained cervical cell images [7]. These techniques lead to successful results only when nuclei are non-overlapping.

In this work, we present an automated gland and nuclei segmentation scheme for prostate and breast histopathology which utilizes a combination of low-level, high-level, and domain-specific information. A Bayesian classifier is used to generate likelihood scenes of structures of interest in the image based on image intensity and textural information. These scenes are combined with domain knowledge regarding arrangement of histological structures through which structural constraints are imposed. A level set algorithm and template matching scheme are then used for gland boundary and nuclear segmentation, respectively. Using the extracted gland boundary, multiple morphological features including area, smoothness, and compactness are extracted. Nuclear centroids are used to extract architectural features via three different graph algorithms including Voronoi, Delaunay triangulation, and minimum spanning tree (MST). Our segmentation algorithm is employed for three different applications: (a) classifying intermediate grades (3 and 4) of prostate cancer, (b) discriminating cancer from non-cancer in breast histology images, and (c) distinguishing Bloom-Richardson

*Thanks to the Coulter Foundation, Aresty Research Center, Cancer Institute of New Jersey, New Jersey Commission on Cancer Research, the National Cancer Institute and the Society for Imaging Informatics in Medicine for providing funding to make this work possible.

low grade (5, 6) breast cancer from high grade (7, 8) breast cancer. Evaluation of the algorithm is done by comparing the classification accuracies obtained for breast and prostate cancer grading and benign versus cancer discrimination with corresponding classification accuracies obtained via manual detection and segmentation of glands and nuclei.

The rest of this paper is organized as follows. Our segmentation algorithm is described in Section 2, and the evaluation results of the algorithm in three different applications (breast and prostate cancer grading and benign versus breast cancer discrimination) are presented in Section 3. Concluding remarks are presented in Section 4.

2. INTEGRATED LOW-, HIGH-LEVEL AND CONTEXTUAL SEGMENTATION MODEL

2.1. System Overview

A flowchart describing our segmentation algorithm and its applications in breast and prostate cancer detection and grading is shown in Figure 1.

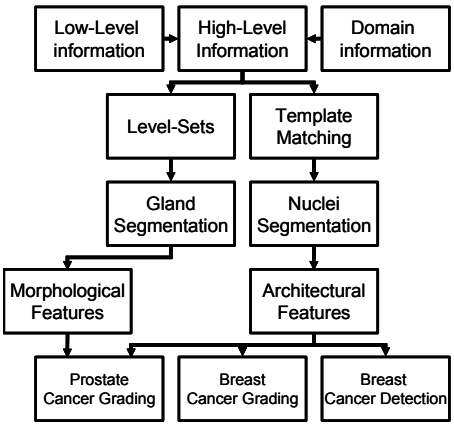

Fig. 1. Flowchart illustrating the system overview.

2.2. Low-level Information

We denote a tissue region by a digital image $\mathcal{C} = (C, f)$ where C is a 2D grid of image pixels $c \in C$ and f is a function that assigns a pixel value (representing the red, blue, and green channels of the RGB space) to c. A training set $\mathcal{S}_v$ of pixels representing a structure of interest v (lumen (L), cytoplasm (S), nuclei (N), etc.) is obtained. The color values $f(c)$ of pixels $c \in \mathcal{S}_v$ are used to generate probability density functions $p(c, f(c)|v)$, where v represents the image class. For each image $\mathcal{C}$, Bayes Theorem is used to obtain a pixel-wise likelihood for each pixel $c \in C$, where $P(v|c, f(c))$ is the probability that c belongs to class v given image pixel value $f(c)$ and obtained as,

$$P(v|c, f(c)) = \frac{P(v)p(c, f(c)|v)}{\sum_{u\in\{L,N,S\}} P(u)p(c, f(c)|u)}, \qquad (1)$$

where $v \in \{L, N, S\}$, $p(c, f(c))|v)$ is the *a priori* conditional probability obtained during training for class v, and $P(v)$ is the prior probability of occurrence for each class v (assumed as non-informative priors). These pixel-wise likelihoods generate a likelihood scene $\mathcal{L}_v$, where the intensity in the likelihood image is the probability of pixel c belonging to class v.

2.3. High-level Information

We consider two shape based approaches for segmentation including: (a) level set and (b) template maching.

2.3.1. Level Set Segmentation

Boundary segmentation is performed using level-sets which makes use of neighboring pixels during evolution of the contour to find the target boundary. A boundary $\mathcal{B}$ evolving in time t and in the 2D space defined by the grid of pixels C is represented by the zero level set $\mathcal{B} = \{(x, y)|\phi(t, x, y) = 0\}$ of a level set function ϕ, where $c = (x, y)$. The evolution of ϕ is then described by a level-set formulation adopted from [8]:

$$\frac{\partial\phi}{\partial t} + F|\nabla\phi| = 0 \qquad (2)$$

where the function F defines the speed of the evolution. The curve evolution is driven by the likelihood image $\mathcal{L}_v$, where $v \in \{L, N, S\}$. The initial contour $\phi_0 = \phi(0, x, y)$ is automatically initialized using low-level information via Bayesian classifier. The algorithm is run until the difference in the contours of one iteration to the next is below an empirically determined threshold.

2.3.2. Template matching

Template matching [9] is done on a binary image ($\mathcal{I}_B$) converted from the likelihood scene $\mathcal{L}_v$. Correlation between the selected template and $\mathcal{I}_B$ is computed at each of the pixels $c \in C$. The choice of template is motivated by the size and shape of the structure of interest. For our application to detection of nuclei, we have chosen four binary elliptical templates with different major and minor axes.

2.4. Incorporating Domain-specific Constraints

Our segmentation algorithm exploits domain-specific information in the form of specific arrangement and relationships between histological structures. For instance, a gland (Fig.2) comprises three main structures of interest: lumen, cytoplasm, and nuclei. The structures are arranged in a specific fashion (lumen is surrounded by cytoplasm, which is surrounded by a ring of nuclei). We exploit the fact that a lumen area needs to be surrounded by cytoplasm, which is then surrounded by a ring of nuclei to constitute a gland.

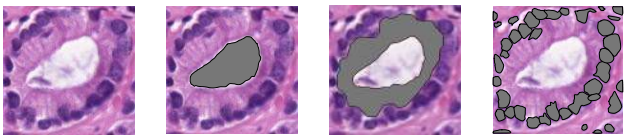

(a) (b) (c) (d)

Fig. 2. Illustration of different regions of interest within a gland (a) Shown outlined in black are the (b) lumen area, (c) cytoplasm, and (d) nuclei.

2.5. Gland Segmentation

A. Low-level Information

Step 1: Bayesian classification of lumen, stroma, nuclei: Low-level image intensity information is used to generate the likelihood scenes $\mathcal{L}_L$, $\mathcal{L}_S$, and $\mathcal{L}_N$ for the lumen, cytoplasm and the nuclei, respectively.

Step 2: Detection of lumen objects: Once the likelihood scenes are generated, we focus on $\mathcal{L}_L$. We define an object O as a

set of contiguous pixels in the lumen likelihood image above an empirically determined threshold. The probability that any object O actually does correspond to lumen is computed as $\boldsymbol{P}_B = \frac{1}{|O|}\sum_{c\in O} P(l|c, f(c))$, where $|O|$ is the cardinality of set O.

Step 3: Removal of false lumen regions based on area: A *priori* knowledge of gland sizes (learnt during offline training phase) is used to identify and remove potential false positives. The *a priori* distribution for the lumen area ($P(O \hookrightarrow l|\mathbf{A})$) is used to assign each object a posterior probability $\boldsymbol{P}_S$ that O corresponds to lumen, where $A = |O|$.

B. Structural Constraints

Step 4: Remove false lumen regions based on surrounding structure: Non-gland regions are eliminated by ensuring that the structure of the gland is as shown in Figure 2. The likelihood scene generated for cytoplasm is used to check for presence of the epithelial cytoplasm surrounding detected lumen regions. The percentage of pixels surrounding the lumen that are above an empirically determined probability within $\mathcal{L}_S$ is calculated as $\boldsymbol{P}_G$.

Step 5: Finding true lumen objects: The joint probability that the object O identified as lumen actually belongs to a gland is given as the product of the independent probabilities $\boldsymbol{P}_B$, $\boldsymbol{P}_S$, and $\boldsymbol{P}_G$: $\boldsymbol{P}(O \hookrightarrow l|\boldsymbol{P}_B, \boldsymbol{P}_S, \boldsymbol{P}_G) = \prod_{\alpha\in\{B,S,G\}} \boldsymbol{P}_\alpha$, where $\hookrightarrow l$ denotes membership in class l. Only those objects with a joint conditional probability over a pre-determined threshold are considered.

C. High-level Information

Step 6: Boundary segmentation: Once the gland lumen has been detected, gland boundary segmentation is performed using level-sets. Curve evolution is driven by $\mathcal{L}_N$ and the initial contour $\phi_0 = \phi(0, x, y)$ is initialized automatically using O found in step 5 above. The curve is evolved outward from O within $\mathcal{L}_N$. Finally, the lumen and nuclear boundaries are extracted from true gland regions.

2.6. Nuclear Segmentation

A. Low-level Information

Step 1: Bayesian classification of nuclei: Low-level image intensity information is used to generate likelihood scene $\mathcal{L}_N$.

Step 2: Convert $\mathcal{L}_N$ to binary image: $\mathcal{L}_N$ is thresholded to a binary image $\mathcal{I}_B = (C, h)$, where $h(c) \in \{0, 1\}$. Let B denote the set of pixels in the background, so that $h(b) = 0$ for all $b \in B$ and $h(c) = 1$ for all $c \in C, c \notin B$.

B. Structural Constraints

Step 3: Euclidean distance transform (EDT): EDT operation [10] is applied on $\mathcal{I}_B$, which transforms into a grey level image $\mathcal{D}_B = (C, f_B)$ where for $c \in C$, $f_B(c)$ is the Euclidean disance to the nearest $b \in B$. The EDT for all pixels $c \in C$ is defined as:

$$f_B(c) = \min_{b\in B}[\mathbf{d}(c, b)] \tag{3}$$

where $\mathbf{d}(c, b)$ is the Euclidean distance betweeen pixels $c, b \in C$. By limiting the template matching to only those pixels $c \in C$ for which $f_B(c) > \lambda$, where λ is some pre-defined threshold, significantly increases the computational speed and efficiency of our algorithm.

C. High-level Information

Step 4: Template matching to detect nuclei: For each $c \in \mathcal{D}_B$ for which $f_B > \lambda$, template matching with 4 templates T_1, T_2, T_3, T_4 is done. The idea is to focus on pixels $c \in \mathcal{D}_B$ for which f_B is high since these are the points that lie close to medial axis of object of interest. At $c \in C$, where $f_B(c) > \lambda$, $\max_j[corr(c, T_j)]$ is computed where $corr(c, T_j)$ is correlation obtained by placing centroid of T_j on c, for $j \in \{1, 2, 3, 4\}$. Thus we obtain a new scene $\varphi^n = (C, f^T)$ where for each $c \in C$, $f^T(c) = \max_j[corr(c, T_j]$. Nuclear centroids are determined as those for which $f^T(c) > \delta$.

3. PROSTATE AND BREAST CANCER GRADING

3.1. Feature Extraction

Following gland and nuclear segmentation, we calculate 8 boundary features from the interior nuclear and lumen boundaries, giving a total of 16 morphological features which quantify the size and shape of the glands [11]. We also calculate 51 graph-based features from Voronoi diagrams, minimum spanning tree, and Delaunay triangulation using the centroids of the nuclei to quantify the spatial relationships of nuclei [3]. The features were chosen based on features used by pathologists in detecting and grading cancer in practice. The goal of our segmentation algorithm is high classification accuracy in distinguishing cancer grades and cancer detection, so to compare our algorithm with manual segmentations, we extract each set of features twice using manual and automatic segmentation. These two feature sets were used in a support vector machine classifier to compare manual and automated segmentations in terms of classifier accuracy. Experiments using our algorithm are described in the next three sub-sections.

3.2. Application A: Prostate Cancer Grading

We seek to classify a database of prostate images containing 16 Gleason grade 3 images, 11 grade 4 images, and 17 benign epithelial images of biopsy tissue. We ran experiments to discriminate between (a) benign epithelium and grade 3, (b)benign epithelium and grade 4, and (c) grade 3 and grade 4 using gland morphology features. The feature set is first reduced using graph embedding, a non-linear dimensionality reduction method, and a support vector machine (SVM) classifier is used for classification in the reduced dimensional space. Accuracies are listed in Table 1, where similar performance between manual and automatic segmentation is observed. Sample results from gland segmentation are shown in Fig. 3(a-e). Fig. 3(e) shows a scatter plot of benign and Gleason grade 4 tissue represented in a three dimensional space obtained through graph embedding.

3.3. Application B: Breast Cancer Detection

We discriminate cancer from non-cancer in breast histology images using architectural features. The dataset contains a total of 18 benign images and 36 cancer images. The feature set is reduced using principal component analysis (PCA) and a SVM classifier is used for classification. We obtain an accuracy of 81.91% using automatic segmentation and 77.10% with manually segmented structures (Table 1), indicating comparable performace between manual and automatic segmentation. A sample cancer image is shown in Fig. 3(f). Graphs are constructed from nuclear centroids identified automatically by our algorithm (Fig.3(i) shows the Voronoi Diagram as an example). A scatter plot representing the cancer and non-cancer images is shown in Fig. 3(j).

3.4. Application C: Breast Cancer Grading

We seek to distinguish 21 images of low-grade breast cancer (grades 5 and 6 on the Bloom-Richardson scale) from 9 images of high-grade cancer (7 and 8). As in the prostate cancer grading example, graph-based features are used to classify high grade vs. low grade cancer. The feature set is reduced using PCA and classification is done using a SVM classifier. The classification accuracies are shown in Table 1 and figures as those for Application B are shown in Fig. 3 (k-o) for a tissue image with a grade 8 breast cancer.

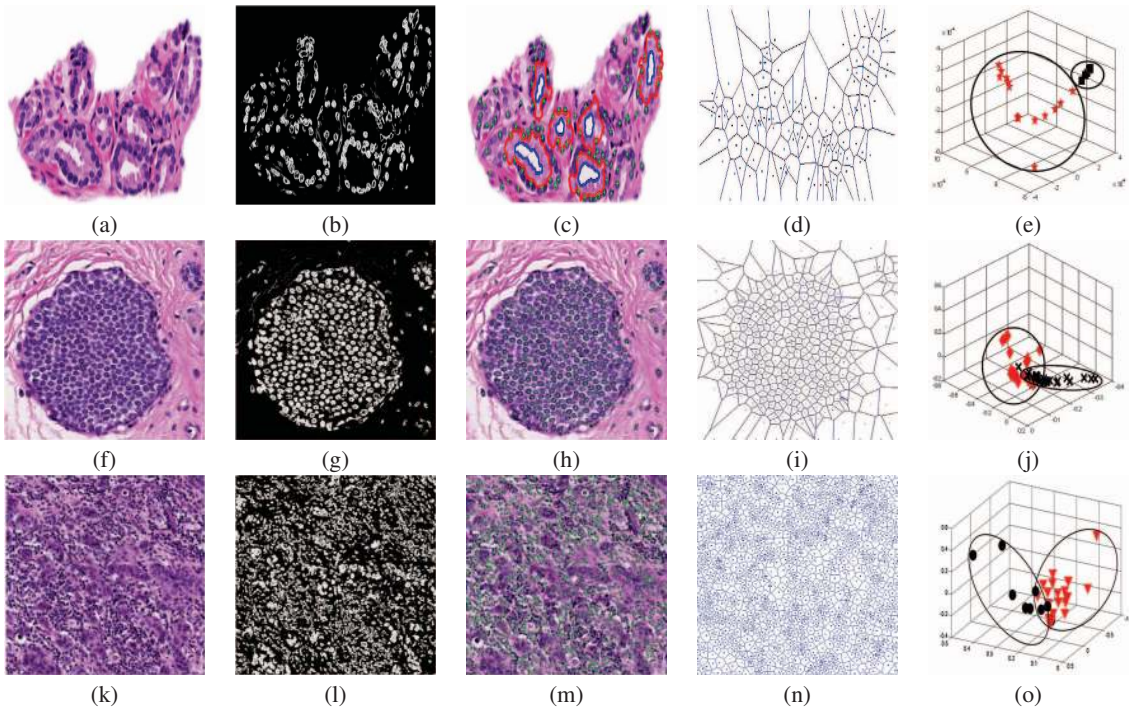

Fig. 3. Tissue images corresponding to (a) Gleason grade 3 prostate cancer, (f) Bloom-Richardson grade 5 and (k) grade 8 cancer. $\mathcal{L}_N$ for (a), (f), (k) are shown in (b), (g), and (l). Segmented gland boundaries and nuclei centroids are shown in (c), (h), and (m). Voronoi diagrams used to generate architectural features are shown in (d), (i), and (n). Distinction between benign tissue (black squares) and grade 4 prostate cancer tissue (red stars) is shown in the reduced 3 dimensional space in the scatter plot in (e). Scatter plots in (j) and (o) show clusterings from cancer(red diamonds) vs. non-cancer(black crosses), and high grade(black circles) vs. low-grade(red triangles) breast cancer, respectively.

Tissue Type	Task	Automated	Manual
Prostate	Grade 3 vs. Grade 4	95.19%	80.76%
	Grade 3 vs. Benign	86.35%	95.14%
	Grade 4 vs. Benign	92.90%	95.14%
Breast	Cancer vs. Non-cancer	81.91%	77.10%
Breast	High vs. Low Grade	80.52%	93.33%

Table 1. SVM classification accuracy for the three applications using the automatically and manually extracted feature sets. Accuracies are averaged over 10 trials using randomized cross-validation.

4. CONCLUDING REMARKS

In this paper, we have demonstrated an integrated nuclear and gland segmentation and detection scheme. The strength of the model is derived from the fact that it incorporates low-, high-level knowledge, and structural constraints imposed via domain knowledge. Morphological and architectural attributes derived from the segmented nuclei and glands were used for (a) grading of prostate cancer, (b) discriminating cancer from non-cancer in breast histology, and (c) discriminating low grade from high grade breast cancer. The corresponding classification accuracies obtained for case (a) were 95.19% for grade 3 vs. grade 4, 86.35% for grade 3 vs. benign, and 92.90% for grade 4 vs. benign; for case (b) was 81.91% and for case (c) was 80.52%. These accuracies compare favourably with the corresponding results obtained via manual segmentation. Future work will focus on evaluating our methods on a larger cohort of images.

5. REFERENCES

[1] HJG. Bloom and WW. Richardson, "Histological grading and prognosis in breast cancer," *British Journal of Cancer*, vol. 11, pp. 359–377, 1957.

[2] R. Montironi, R. Mazzuccheli, et al., "Gleason grading of prostate cancer in needle biopsies or radical prostatectomy specimens: contemporary approach, current clinical significance and sources of pathology discrepencies," *BJU Int.*, vol. 95, no. 8, pp. 1146–1152, 2005.

[3] S. Doyle, M. Hwang, K. Shah, A. Madabhushi, et al., "Automated grading of prostate cancer using architectural and textural image features," *IEEE ISBI*, pp. 1284–1287, 2007.

[4] L. Latson, B. Sebek, and K. Powell, "Automated cell nuclear segmentation in color images of hematoxylin and eosin-stained breast biopsy," *Analytical and Quantitative Cytology and Histology*, vol. 25, no. 6, pp. 321–331, 2003.

[5] S. Petushi, F.U. Garcia, M.M. Haber, et al., "Large-scale computations on histology images reveal grade-differentiating parameters for breast cancer," *BMC Medical Imaging*, vol. 6, no. 14, October 2006.

[6] V.R. Korde, H. Bartels, et al., "Automatic segmentation of cell nuclei in bladder and skin tissue for karyometric analysis," *Biophotonics 2007: Optics in Life Science*, vol. 6633, pp. 6633V, 2007.

[7] P. Bamford and B. Lovell, "Unsupervised cell nucleus segmentation with active contours," *Signal Processing*, vol. 71, pp. 203–213, 1998.

[8] C. Li, C. Xu, C. Gui, and M.D. Fox, "Level set evolution without re-initialization: a new variational formulation," *IEEE CVPR*, vol. 1, pp. 430–436, 2005.

[9] I. Sintorn, M. Homman-Loudiyi, et al., "A refined circular template matching method for classification of human cytomegalovirus capsids in tem images," *Computer Methods and Programs in Biomedicine*, vol. 76, no. 2, pp. 95–102, 2004.

[10] A. Datta and S. Soundaralakshmi, "Fast and scalable algorithms for the euclidean distance transform on a linear array with a reconfigurable pipelined bus system," *Journal of Parallel and Distributed Computing*, vol. 64, pp. 360–369, 2004.

[11] S. Naik, S. Doyle, A. Madabhushi, et al., "Gland segmentation and computerized gleason grading of prostate histology by integrating low-, high-level and domain specific information," *MIAAB Workshop*, 2007.